UCSF
UC San Francisco Previously Published Works

Title

Accelerating PERx reaction enables covalent nanobodies for potent neutralization of SARS-CoV-2 and variants

Permalink

https://escholarship.org/uc/item/8571p4gb

Journal

Chem, 8(10)

ISSN

1925-6981

Authors

Yu, Bingchen
Li, Shanshan
Tabata, Takako
et al.

Publication Date

2022-10-01

DOI

10.1016/j.chempr.2022.07.012

Peer reviewed

eScholarship.org Powered by the California Digital Library
University of California

Since January 2020 Elsevier has created a COVID-19 resource centre with free information in English and Mandarin on the novel coronavirus COVID-19. The COVID-19 resource centre is hosted on Elsevier Connect, the company's public news and information website.

Elsevier hereby grants permission to make all its COVID-19-related research that is available on the COVID-19 resource centre - including this research content - immediately available in PubMed Central and other publicly funded repositories, such as the WHO COVID database with rights for unrestricted research re-use and analyses in any form or by any means with acknowledgement of the original source. These permissions are granted for free by Elsevier for as long as the COVID-19 resource centre remains active.

Chem

CellPress

Article

Accelerating PERx reaction enables covalent nanobodies for potent neutralization of SARS-CoV-2 and variants

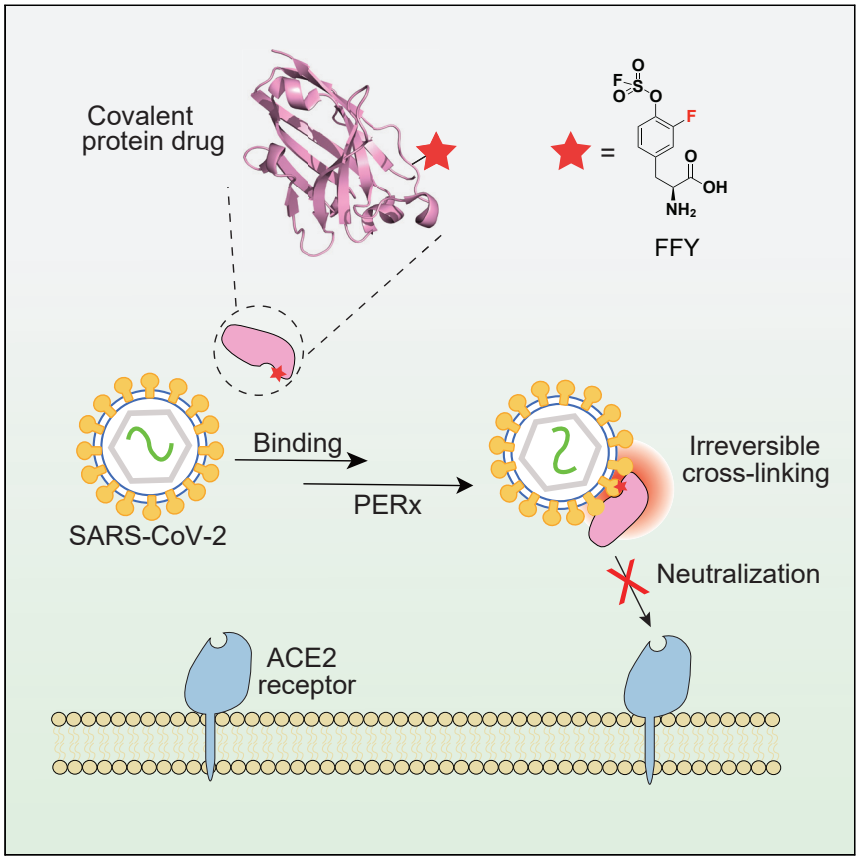

Traditional nanobodies interact with their targets reversibly, leading to dissociation and incomplete inhibition. Wang and co-workers have designed a latent bioreactive amino acid (FFY) and genetically encoded it into nanobodies. Upon nanobody binding to the viral spike protein, FFY covalently reacts with spike via a proximity-enabled reactive therapeutic (PERx) mechanism, enabling the nanobody to bind to SARS-CoV-2 irreversibly and effectively block viral infection. The FFY-incorporated covalent nanobodies neutralized both wild-type SARS-CoV-2 and its various variants with drastically higher potency than the noncovalent wild-type nanobodies.

Bingchen Yu, Shanshan Li, Takako Tabata, ..., Jun Liu, Melanie Ott, Lei Wang

lei.wang2@ucsf.edu

Highlights

Bioreactive Uaa FFY exhibits faster cross-linking kinetics than its predecessor, FSY

FFY enables nanobodies to bind with SARS-CoV-2 spike covalently and irreversibly

FFY incorporation drastically increases nanobodies' potency in viral neutralization

FSY-engineered human ACE2 receptor binds to SARS-CoV-2 spike covalently

Yu et al., Chem *8*, 1–18
October 13, 2022 © 2022 Elsevier Inc.
https://doi.org/10.1016/j.chempr.2022.07.012

Please cite this article in press as: Yu et al., Accelerating PERx reaction enables covalent nanobodies for potent neutralization of SARS-CoV-2 and variants, Chem (2022), https://doi.org/10.1016/j.chempr.2022.07.012

Chem

CellPress

Article

Accelerating PERx reaction enables covalent nanobodies for potent neutralization of SARS-CoV-2 and variants

Bingchen Yu,[1,4] Shanshan Li,[1,4] Takako Tabata,[2] Nanxi Wang,[1] Li Cao,[1] G. Renuka Kumar,[2] Wei Sun,[1] Jun Liu,[1] Melanie Ott,[2,3] and Lei Wang[1,5,*]

SUMMARY

The long-lasting COVID-19 pandemic and increasing SARS-CoV-2 variants demand effective drugs for prophylactics and treatment. Protein-based biologics offer high specificity, yet their noncovalent interactions often lead to drug dissociation and incomplete inhibition. Here, we have developed covalent nanobodies capable of binding with SARS-CoV-2 irreversibly via a proximity-enabled reactive therapeutic (PERx) mechanism. A latent bioreactive amino acid (FFY) was designed and genetically encoded into nanobodies to accelerate the PERx reaction rate. Compared with the noncovalent wild-type nanobody, the FFY-incorporated covalent nanobodies neutralized both wild-type SARS-CoV-2 and its Alpha, Delta, Epsilon, Lambda, and Omicron variants with drastically higher potency. This PERx-enabled covalent-nanobody strategy and the related insights into increased potency can be valuable to developing effective therapeutics for various viral infections.

INTRODUCTION

In December 2019, a novel coronavirus (SARS-CoV-2) caused an outbreak of coronavirus disease 2019 (COVID-19),[1] which has been ongoing for over 2 years and has resulted in an unprecedented burden to public health globally. In addition to vaccines,[2] incessant efforts have been spent on developing drugs to inhibit the virus both prophylactically and as treatment. Because cell entry of SARS-CoV-2 depends on the binding of the viral spike protein to the human cellular angiotensin-converting enzyme 2 (ACE2) receptor,[3,4] various types of reagents have been developed to block the spike-ACE2 interaction to neutralize SARS-CoV-2.[5–12] Despite the exciting progress, complete inhibition of SARS-CoV-2 infection remains challenging. Biologics such as protein-based drugs exert their function through noncovalent interactions, which are reversible to allow drug dissociation such that the unblocked virus can re-access and infect cells. In addition, rapid evolution of the SARS-CoV-2 RNA genome has led to variants that escape neutralization by the human immune system or various noncovalent reagents.[13–15] Covalent small-molecule drugs have been shown to possess enhanced potency, prolonged duration of action, and the ability to mitigate drug resistance.[16,17] We thus envisioned that protein drugs able to bind the virus irreversibly in covalent mode would be highly desirable to attain potent and complete inhibition of viral infection, as well as to minimize viral escape through mutation. However, whether and how covalent protein drugs can increase potency in neutralizing viral infection await exploration.

THE BIGGER PICTURE

The long-lasting COVID-19 pandemic and increasing SARS-CoV-2 variants demand effective therapeutic strategies. Herein, we have engineered unique unnatural amino acids into proteins and developed covalent nanobodies capable of irreversibly binding with the viral spike protein. These covalent nanobodies are able to neutralize both SARS-CoV-2 and its different variants with drastic higher potency than traditional nanobodies, affording a potential prophylactic and medication for COVID-19. In addition, our strategy could provide an original general route to developing effective therapeutics for various other viral infections, such as influenza, hepatitis, AIDS, and anthrax.

Please cite this article in press as: Yu et al., Accelerating PERx reaction enables covalent nanobodies for potent neutralization of SARS-CoV-2 and variants, Chem (2022), https://doi.org/10.1016/j.chempr.2022.07.012

Natural proteins generally lack the ability to bind with a target covalently.[18,19] To break this natural barrier, we recently reported a proximity-enabled reactive therapeutics (PERx) strategy for generating covalent protein drugs.[20,21] A latent bioreactive unnatural amino acid (Uaa) is incorporated into the protein drug through expansion of the genetic code,[22] which reacts with a natural residue on the target only upon drug-target binding, realizing specific cross-linking of the drug to the target covalently. We have demonstrated that a covalent PD-1 drug efficiently inhibits tumor growth in mice with therapeutic efficacy superior to that of an FDA-approved antibody.[20] This initial success was achieved on suppression of tumor growth, which is a relatively long process on the order of days to weeks. It remains to be established whether PERx can be generally applicable to other proteins for enhanced efficacy and to acute processes requiring fast and prompt reaction.

Here, we have developed covalent nanobodies to irreversibly inhibit the infection of both SARS-CoV-2 and its variants via the PERx principle. To cope with acute viral infection, we designed a latent bioreactive Uaa, fluorine-substituted fluorosulfate-L-tyrosine (FFY), and genetically encoded it to accelerate the PERx reaction rate by 2.4-fold over the original FSY, enabling fast cross-linking within 10 min. Consequently, FFY-based nanobodies exhibited a drastic potency increase in neutralizing SARS-CoV-2 (41-fold), as well as its Alpha (23-fold), Delta (39-fold), Epsilon (38-fold), Lambda (24-fold), and Omicron (8- to 10-fold) variants. Using the PERx strategy, we also generated covalent soluble human ACE2 to bind to the spike protein irreversibly. This PERx-based covalent-nanobody strategy could provide a unique route to developing effective therapeutics for viral infections.

RESULTS

Covalent nanobodies to neutralize SARS-CoV-2 via PERx

Nanobodies (single-domain antibodies) are generally heat stable, easily produced in bacteria, and small (~15 kDa) to increase the density of inhibitory domains for efficient blockage[8] and can be humanized to minimize potential immunogenicity. Multiple groups have selected nanobodies that bind to the spike protein with high affinities and show promising inhibition against SARS-CoV-2 infection of Vero cells or ACE2-expressing HEK-293 cells.[7,23,24] Our strategy was to genetically incorporate a latent bioreactive Uaa into the nanobody that specifically binds to the receptor binding domain (RBD) of the SARS-CoV-2 viral spike protein (Figure 1A). Upon binding of the nanobody with the spike RBD, the latent bioreactive Uaa would be brought into close proximity to a target residue of the spike RBD, which would enable the Uaa to react with the target residue specifically, irreversibly cross-linking the nanobody with the spike RBD. The bound nanobody would prevent the spike RBD from interacting with the human ACE2 receptor, blocking viral infection. The resultant covalent nanobody would thus function as a PERx. Compared with conventional nanobodies, which bind in noncovalent mode and are in dynamic association and dissociation with the spike RBD, covalent nanobodies would permanently bind to the spike RBD and neutralize the virus with enhanced potency (Figure 1B).

Genetically encoding FSY to generate covalent nanobodies that bind to the spike RBD irreversibly *in vitro*

We initially chose to use the latent bioreactive Uaa FSY for its stability and ability to react with Tyr, His, or Lys via a proximity-enabled sulfur fluoride exchange (SuFEx) reaction under biocompatible and cellular conditions (Figure 2A).[25] On the basis of the crystal structure of the human SARS-CoV-2 spike RBD in complex with nanobody H11-D4,[23] nanobody MR17-K99Y,[24] or nanobody SR4,[24] we decided to incorporate FSY at site R27, S30, E100, W112, D115, or Y116 of nanobody H11-D4

[1]Department of Pharmaceutical Chemistry and Cardiovascular Research Institute, University of California, San Francisco, San Francisco, CA 94158, USA

[2]Gladstone Institutes, San Francisco, CA 94158, USA

[3]Department of Medicine, University of California, San Francisco, San Francisco, CA 94158, USA

[4]These authors contributed equally

[5]Lead contact

*Correspondence: lei.wang2@ucsf.edu

https://doi.org/10.1016/j.chempr.2022.07.012

Please cite this article in press as: Yu et al., Accelerating PERx reaction enables covalent nanobodies for potent neutralization of SARS-CoV-2 and variants, Chem (2022), https://doi.org/10.1016/j.chempr.2022.07.012

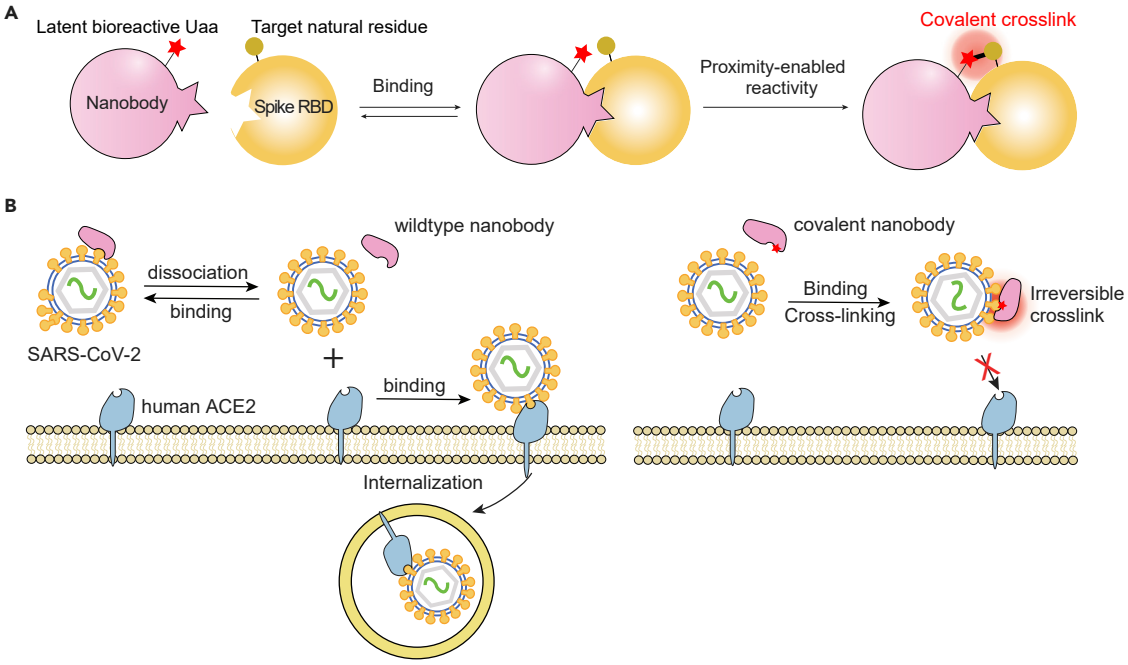

Figure 1. Covalent nanobodies irreversibly inhibit SARS-CoV-2 infection via PERx

(A) The PERx principle of developing covalent nanobodies to irreversibly bind with the spike RBD. Only upon nanobody binding with the spike RBD can the latent bioreactive Uaa react with the target natural residue, covalently cross-linking the nanobody with the spike RBD.

(B) Whereas the conventional nanobody can dissociate from the spike RBD, the covalent nanobody binds with the spike RBD irreversibly, permanently preventing viral binding with ACE2 receptor and thus blocking infection more effectively.

(Figure 2B), site Y99 or D101 of nanobody MR17-K99Y (Figure 2C), and site Y37, H54, or S57 of nanobody SR4 (Figure 2D), respectively. Western blot analysis of lysates of *E. coli* cells expressing these mutant nanobody genes and the $tRNA^{Pyl}$/FSYRS pair[25] confirmed that FSY was successfully incorporated into the nanobodies in the presence of FSY (Figure S1). Wild-type (WT) and FSY-incorporated nanobodies were purified with affinity chromatography. The yield for SR4(57FSY) was 2.4 mg/L, and other FSY mutants had similar yields. Mass spectrometry (MS) analysis of the intact SR4(57FSY) protein confirmed that FSY was incorporated into SR4 at site 57 with high fidelity (Figure 2E).

To test whether FSY-incorporated nanobodies could bind to the spike RBD covalently *in vitro*, we incubated 2.5 μM WT nanobodies or their FSY mutants with 0.5 μM spike RBD at 37°C for 12 h and then performed western blot analysis under denatured conditions (Figures 2F–2H). As expected, none of the three WT nanobodies formed a covalent complex with the spike RBD. A stable covalent complex was detected for H11-D4(115FSY) and H11-D4(116FSY) with low cross-linking efficiencies (Figure 2F), for MR17-K99Y(101FSY) with a 10.5% cross-linking efficiency (Figure 2G), for SR4(54FSY) with a 28.3% cross-linking efficiency, and for SR4(57FSY) with a 41.3% cross-linking efficiency (Figure 2H). We then further studied time-dependent cross-linking of the spike RBD with SR4(54FSY) or SR4(57FSY) nanobodies, which showed that SR4(57FSY) was more efficient (Figures 2I and 2J). SR4(57FSY) was thus used in subsequent experiments.

SR4(57FSY) inhibits binding of the spike RBD to cell-surface ACE2 receptor

We next tested the efficacy of SR4 nanobodies to inhibit the binding of the spike RBD-mFc (a mouse Fc tag appended at the C terminus of the spike RBD) to

Please cite this article in press as: Yu et al., Accelerating PERx reaction enables covalent nanobodies for potent neutralization of SARS-CoV-2 and variants, Chem (2022), https://doi.org/10.1016/j.chempr.2022.07.012

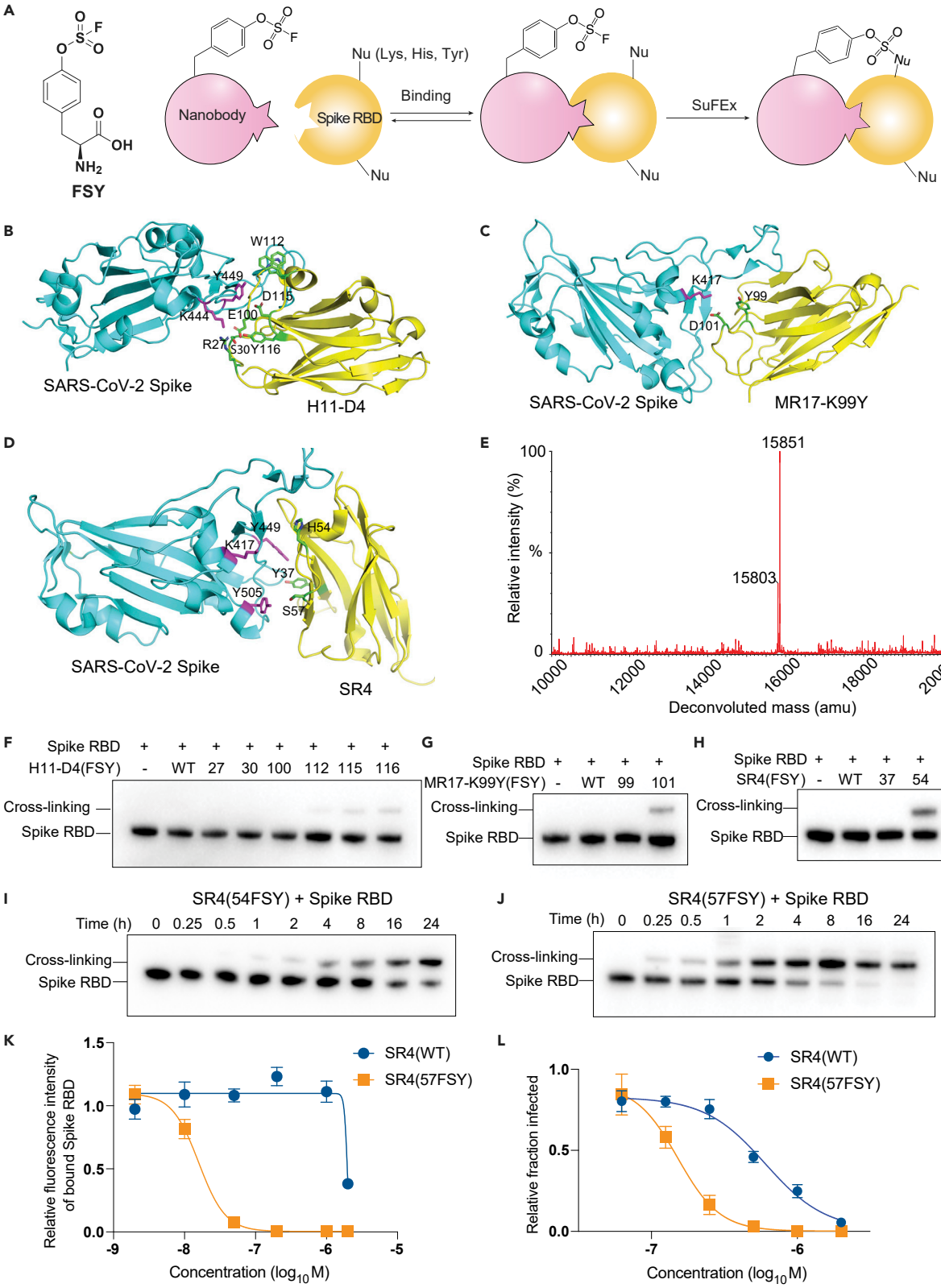

Please cite this article in press as: Yu et al., Accelerating PERx reaction enables covalent nanobodies for potent neutralization of SARS-CoV-2 and variants, Chem (2022), https://doi.org/10.1016/j.chempr.2022.07.012

Figure 2. FSY-incorporated covalent nanobodies cross-link the spike RBD and more potently inhibit spike RBD binding with cell-surface ACE2, as well as pseudoviral infection

(A) Structure of FSY and its proximity-enabled SuFEx reaction with Lys, His, or Tyr for PERx.

(B–D) Crystal structure of nanobodies in complex with the SARS-CoV-2 spike RBD: (B) nanobody H11-D4 (PDB: 6YZ5), (C) nanobody MR17-K99Y (PDB: 7CAN), and (D) nanobody SR4 (PDB: 7C8V). Sites selected for FSY incorporation in the nanobodies and intended target residues of the spike RBD are shown in green and magenta sticks, respectively.

(E) Electrospray ionization mass spectrometry (ESI-MS) of the intact SR4(57FSY) confirms FSY incorporation. Expected: 15,802.5 Da; observed: 15,803 Da. The peak observed at 15,851 Da corresponded to SR4(57FSY) with cysteine oxidation.

(F–H) Cross-linking of the spike RBD with WT nanobody H11-D4 (F), MR17-K99Y (G), SR4 (H), and their FSY mutants at 37°C for 12 h. Mouse Fc tag appended at the C terminus of the spike RBD was detected in the western blot.

(I and J) Western blot analysis of 5 μM SR4(54FSY) or SR4(57FSY) cross-linking with 0.5 μM spike RBD at the indicated time points.

(K) Inhibition curve of the spike RBD-mFc binding to 293T-ACE2 cells by SR4(WT) or SR4(57FSY). SR4(WT) or SR4(57FSY) (in a final concentration of 2, 1, 0.2, 0.05, 0.01, and 0.002 μM) was used to inhibit 10 nM spike RBD-mFc binding to 293T-ACE2 cells. Fluorescence intensity representing the spike RBD-mFc bound to 293T-ACE2 cells was measured with FITC-labeled mFc antibody by flow cytometry. Error bars represent the SD; n = 3 biological replicates.

(L) Inhibition of SARS-CoV-2 pseudovirus infection of 293T-ACE2 cells by SR4(WT) or SR4(57FSY). The percentage of GFP-positive cells, the indicator of infection, was measured with flow cytometry. The normalized infection in the y axis was calculated as (the percentage of GFP-positive cells infected by nanobody-treated pseudovirus)/(the percentage of GFP-positive cells infected by pseudovirus only). Error bars represent the SD; n = 3 biological replicates.

See also Figure S1.

293T-ACE2 cells, a HEK293T cell line stably expressing human ACE2 protein on the cell surface. We individually incubated different concentrations of SR4(WT) or SR4(57FSY) with the spike RBD-mFc at 37°C for 12 h to allow cross-linking and then incubated them with 293T-ACE2 cells for 1 h. After incubation, cells were stained with FITC-labeled anti-mFc and analyzed with flow cytometry (Figure 2K). As expected, SR4(WT) bound to the spike RBD reversibly such that the spike RBD could still bind to ACE2 on the cell surface, resulting in an IC_{50} of 1,980 nM. In contrast, the covalent SR4(57FSY) showed highly efficient blocking of spike RBD binding to 293T-ACE2 cells with an IC_{50} of 15.8 nM (Figure 2K). The IC_{50} of SR4(57FSY) was 125-fold lower than that of SR4(WT), demonstrating the drastic improvement of the covalent nanobody in inhibiting the binding of the spike RBD to cell-surface ACE2 receptor.

SR4(57FSY) neutralizes pseudovirus infection of 293T-ACE2 cells

We next tested the neutralization activity of SR4(WT) or SR4(57FSY) nanobody against SARS-CoV-2 spike pseudotyped lentivirus by using a widely adopted protocol.[26,27] SARS-CoV-2 reporter virus particles display antigenically correct spike protein on a heterologous virus core and carry a modified genome that expresses a convenient GFP reporter gene, which is integrated and expressed upon successful viral entry into cells harboring the ACE2 receptor. In brief, we incubated the pseudoviruses with various concentrations of SR4(WT) or SR4(57FSY) at 37°C for 1 h and subsequently used them to infect 293T-ACE2 cells for 48 h. We then analyzed cells by flow cytometry for GFP signal to determine the percentage of infected cells. The IC_{50} for SR4(WT) was measured to be 602.8 nM (Figure 2L), close to the literature-reported 390 nM,[24] whereas the IC_{50} was measured to be 151.6 nM for SR4(57FSY). This 4-fold decrease in IC_{50} demonstrates that the covalent SR4(57FSY) was more potent in inhibiting pseudovirus infection of ACE2-expressing human cells than SR4(WT), but the enhancement was moderate.

We further tested the neutralization ability of SR4(WT) or SR4(57FSY) nanobody against authentic SARS-CoV-2 infection of ACE2-expressing human cells. Surprisingly, no significant enhancement of SR4(57FSY) over SR4(WT) was measured (data not shown). A variety of nanobodies—differing in affinity, number of the contacting RBD, binding epitope, and state of the RBD—were selected to bind with the

Please cite this article in press as: Yu et al., Accelerating PERx reaction enables covalent nanobodies for potent neutralization of SARS-CoV-2 and variants, Chem (2022), https://doi.org/10.1016/j.chempr.2022.07.012

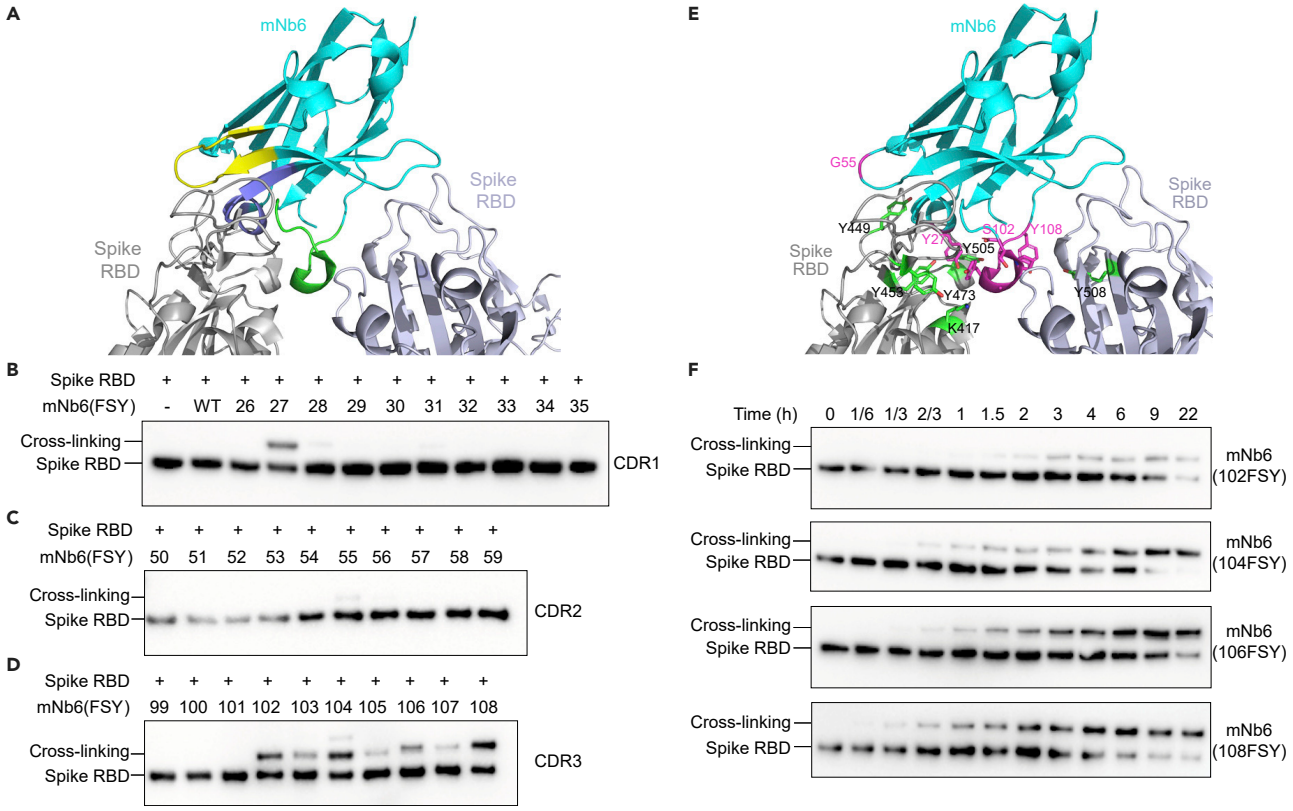

Figure 3. Covalent nanobodies based on mNb6, which binds two spike RBDs

(A) Crystal structure of mNb6 (cyan) binding with two spike RBDs (gray and light blue) (PDB: 7KKL). FSY was individually incorporated at 30 different positions located at the CDR1 (blue), CDR2 (yellow), and CDR3 (green) regions of the nanobody without referring to the specific structure of mNb6.

(B–D) Western blot analysis of cross-linking between the spike RBD and WT mNb6 or FSY mutants located at three CDRs of the nanobody.

(E) Identified FSY cross-linking sites are mapped onto mNb6 in magenta, and potential target residues of the spike RBD are indicated in green (PDB: 7KKL).

(F) Western blot analysis of mNb6(FSY) mutants (5 μM) cross-linking with the spike RBD (0.5 μM) at the indicated time points.

spike protein of SARS-CoV-2. We therefore sought to covalently engineer other nanobodies differing from SR4 in various aspects.

Generating covalent nanobodies from mNb6

In contrast to SR4, which binds a single spike RBD in its up state and has relatively low affinity,[24] nanobody mNb6 contacts two spike RBDs simultaneously in their down state and has higher affinity.[7] To identify which sites of mNb6 would allow covalent cross-linking of the spike RBD, we incorporated FSY individually at 30 different sites located at the three complementarity-determining regions (CDRs) of mNb6 (Figure 3A). Although the crystal structure of mNb6 in complex with RBD is available,[7] we performed this comprehensive site screening to show that for proteins with well-defined regions, such as the nanobody, one could readily determine the appropriate sites for FSY cross-linking without sophisticated high-throughput screening or detailed structures. We incubated 2 μM mNb6(WT) and its FSY mutant proteins with 0.5 μM spike RBD in PBS (pH 7.4) at 37°C for 12 h and then performed western blot analysis (Figures 3B–3D). When FSY was incorporated at site 27 in CDR1, site 55 in CDR2, or sites 102–108 in CDR3, a covalent complex of mNb6 with the spike RBD was detected, indicating that multiple sites in mNb6 allowed covalent cross-linking with the spike RBD. Mapping these cross-linking sites onto the structure of the

Please cite this article in press as: Yu et al., Accelerating PERx reaction enables covalent nanobodies for potent neutralization of SARS-CoV-2 and variants, Chem (2022), https://doi.org/10.1016/j.chempr.2022.07.012

CellPress

mNb6-spike complex showed that there was a targetable Lys or Tyr within the FSY reaction distance (Figure 3E). Interestingly, at multiple cross-linking sites (G55, P103, G106, D107, and Y108), FSY and the target residues did not have their side chains optimally oriented for FSY reaction, so picking these sites for FSY incorporation is not obvious by only inspection of the crystal structure. The cross-linking occurred at these sites possibly because the located loop allowed certain flexibility for side-chain re-orientation. We then performed a kinetic study on the four more efficient sites on CDR3 (Figure 3F) and found that mNb6(108FSY) showed the fastest cross-linking rate. We thus chose site 108 to incorporate Uaa for subsequent experiments.

FFY as a latent bioreactive Uaa to the accelerate PERx reaction rate

The potency of a covalent protein drug would rely on the rate and extent of latent bioreactive Uaa to form a covalent bond with the target residue of the target protein. Because protein interactions are dynamic, a fast reaction rate would be essential to ensure covalent-bond formation before protein dissociation. Given a certain contact time, the reaction extent increases as the reaction rate increases, which can be critical to achieving complete inhibition of viral infection. Introducing electron-withdrawing groups on the aromatic ring has been reported to increase the SuFEx rates.[28] We thus envisioned that adding electron-withdrawing substituents to FSY would accelerate its proximity-enabled reaction rate when used in PERx.

As a result, we designed and evaluated FFY (Figure 4A). We synthesized FFY by using [4-(acetylamino)phenyl]imidodisulfuryl difluoride (AISF)[29] and then deprotected the Boc protecting group with hydrogen chloride. Because FFY and FSY have similar structures, we reasoned that FSYRS, a pyrrolysyl-tRNA synthetase (PylRS) mutant that we previously evolved to incorporate FSY,[25] should be able to incorporate FFY into proteins as well. To test this idea, we co-expressed the enhanced GFP (EGFP) gene containing a TAG codon at permissive site 182 with genes for $tRNA^{Pyl}$/FSYRS in *E. coli*. In the absence of FFY, no obvious fluorescence was detected; in the presence of FFY, fluorescence intensity was measured to increase with FFY concentration (Figure 4B), suggesting FFY incorporation into EGFP. We also co-expressed mNb6(108TAG) with $tRNA^{Pyl}$/FSYRS in *E. coli* and observed that full-length mNb6 was produced in the presence of 2 mM FFY or 1 mM FSY (Figure 4C) in a yield of 1.0 mg/L. mNb6(WT), mNb6 (108FSY), and mNb6(108FFY) proteins were purified with Ni^{2+} affinity chromatography. MS analysis of the intact protein confirmed that FFY was incorporated into mNb6 at site 108 in high fidelity. A major peak observed at 13,721 Da corresponded to intact mNb6(108FFY) (Figure 4D; expected 13,720.7 Da). A minor peak observed at 13,702 Da corresponded to mNb6(108FFY) lacking F, suggesting a slight F elimination during MS measurement.[25] We also verified mNb6(WT) and mNb6(108FSY) via MS analysis of the intact proteins (Figures 4E and S2).

We next tested whether FFY could improve reaction kinetics over FSY. We incubated the spike RBD (0.5 μM) with 5 μM mNb6(108FSY) or mNb6(108FFY) in PBS (pH 7.4) at 37°C for different durations and then performed western blot analysis of the cross-linking. As shown in Figure 4F, mNb6(108FFY) showed an evidently faster rate than mNb6(108FSY) in cross-linking the spike RBD. Covalent cross-linking could be robustly detected within 10 min for mNb6(108FFY) (Figure S3), whereas mNb6(108FSY) took over 20 min. The apparent first-order constant k_{obs} was $0.244 \pm 0.031\ h^{-1}$ (n = 3) for mNb6(108FFY) and $0.102 \pm 0.007\ h^{-1}$ (n = 3) for mNb6(108FSY) (Figure 4F; quantification in Figure S4). Thus, FFY increased

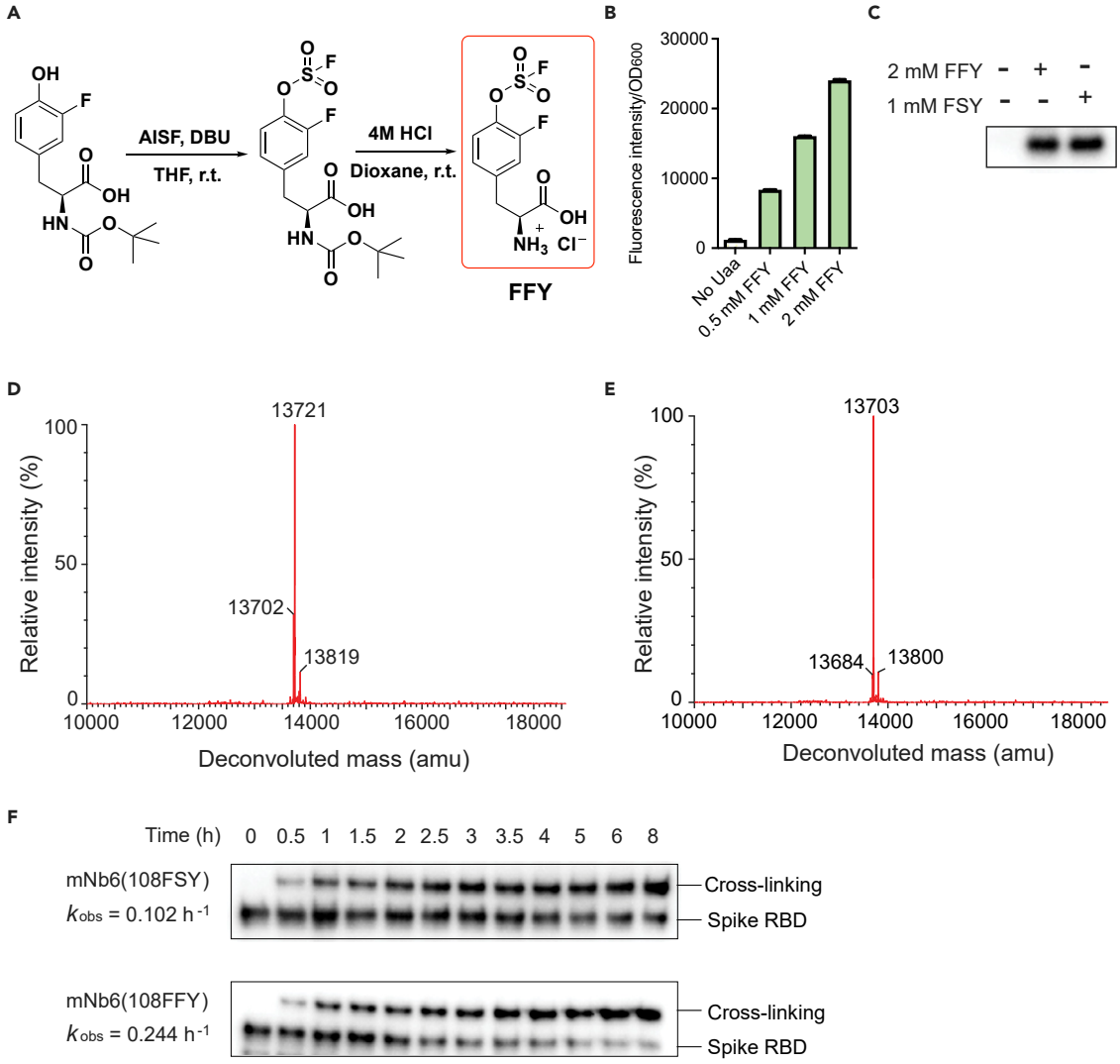

Figure 4. Designing and genetically encoding FFY to accelerate the PERx reaction rate

(A) Chemical synthesis of FFY.

(B) Genetic incorporation of FFY into EGFP at site 182 in *E. coli* with the use of the $tRNA^{PylI}$/FSYRS pair. The fluorescence intensity of cells was measured and normalized by OD_{600}. Error bars represent the SD; n = 3 biological replicates.

(C) Genetic incorporation of FFY or FSY into mNb6 at site 108 in *E. coli* with the use of the $tRNA^{PylI}$/FSYRS pair. Cell lysates were analyzed by western blotting using an anti-Hisx6 antibody.

(D) MS analysis of the intact mNb6(108FFY). Expected: 13,720.7 Da; observed: 13,721 Da.

(E) MS analysis of the intact mNb6(108FSY). Expected: 13,702.7 Da; observed: 13,703 Da. The minor peak at 13,684 Da corresponds to mNb6(108FSY) lacking F, suggesting slight F elimination during MS measurement.

(F) Western blot analysis of cross-linking kinetics indicates that FFY increased the reaction rate to 2.4-fold over FSY. The spike RBD (0.5 μM) was incubated with 5 μM mNb6(108FFY) or mNb6(108FSY) in PBS (pH = 7.4) at 37°C for the indicated time.

See also Figures S2–S5.

the PERx reaction rate over FSY in the mNb6 system to 240%, so we used mNb6(108FFY) for subsequent viral inhibition tests. We also studied the stability of mNb6(108FFY) under relatively long-term storage conditions. The freshly prepared mNb6(108FFY) in PBS was lyophilized and kept under 4°C for 15 days. We then redissolved the lyophilized mNb6(108FFY) powder and found that it cross-linked with the WT spike RBD as efficiently as the freshly prepared mNb6(108FFY) (Figure S5), suggesting the suitability of mNb6(108FFY) for drug development and storage.

Please cite this article in press as: Yu et al., Accelerating PERx reaction enables covalent nanobodies for potent neutralization of SARS-CoV-2 and variants, Chem (2022), https://doi.org/10.1016/j.chempr.2022.07.012

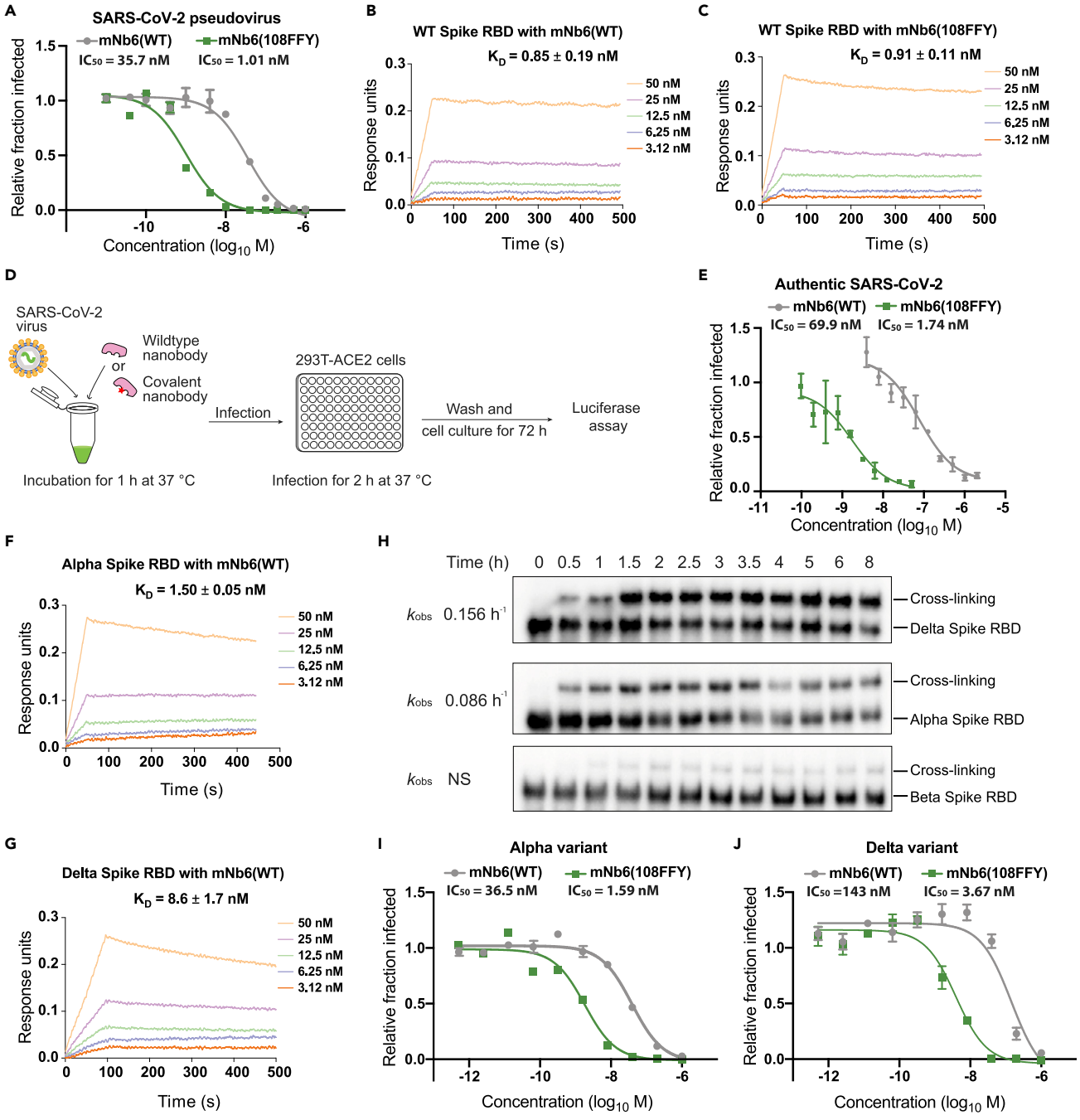

K

SARS-CoV-2 variant	K_D with mNb6(WT) (nM)	mNb6(108FFY) / mNb6(WT) (fold increase)
WT	0.85	36
Alpha	1.50	23
Delta	8.60	39
Epsilon	1.32	38
Lambda	2.86	24

Figure 5. mNb6(108FFY) neutralizes SARS-CoV-2 and certain variants with markedly increased potency over mNb6(WT)

(A) mNb6(108FFY) showed 36-fold higher potency than mNb6(WT) in inhibiting SARS-CoV-2 pseudovirus infection.

(B and C) BLI of mNb6(WT) or mNb6(108FFY) binding to the spike RBD shows no significant difference in K_D.

Please cite this article in press as: Yu et al., Accelerating PERx reaction enables covalent nanobodies for potent neutralization of SARS-CoV-2 and variants, Chem (2022), https://doi.org/10.1016/j.chempr.2022.07.012

Figure 5. *Continued*

(D) Scheme showing procedures for neutralizing authentic SARS-CoV-2 with WT or covalent nanobody.

(E) mNb6(108FFY) showed 41-fold higher potency than mNb6(WT) in inhibiting authentic SARS-CoV-2 infection.

(F and G) BLI of mNb6(WT) binding to the RBD of the Alpha (F) or Delta (G) variant of SARS-Cov-2.

(H) Cross-linking of mNb6(108FFY) with the spike RBD of SARS-CoV-2 variants at the indicated incubation time *in vitro*.

(I) mNb6(108FFY) showed 23-fold higher potency than mNb6(WT) in inhibiting the Alpha variant pseudovirus infection.

(J) mNb6(108FFY) showed 39-fold higher potency than mNb6(WT) in inhibiting the Delta variant pseudovirus infection.

(K) Summary of binding affinity and potency increase in neutralizing SARS-CoV-2 variant pseudoviruses.

For all BLI experiments in (B), (C), (F), and (G), n = 3 biological repeats; K_D is presented as mean ± SD. Representative binding sensorgrams of one sample are shown. For all pseudovirus and authentic SARS-CoV-2 inhibition experiments in (A), (E), (I), and (J), n = 3 biological repeats; error bars represent the SD. See also Figures S6–S10.

mNb6(108FFY) potently neutralizes both pseudovirus and authentic SARS-CoV-2 infection

With FFY's fast kinetics, we tested the efficacy of mNb6(108FFY) in neutralizing lentivirus pseudotyped with the SARS-CoV-2 spike protein. We incubated pseudovirus with varying concentrations of mNb6(108FFY) or mNb6(WT) for 1 h at 37°C and then used the nanobody-pseudovirus mixture to infect 293T-ACE2 cells for 48 h at 37°C. We determined the percentage of cell infection by measuring GFP signal via flow cytometry. The IC_{50} of mNb6(WT) was measured to be 35.7 nM. In contrast, mNb6(108FFY) showed an IC_{50} of 1.0 nM, exhibiting a marked 36-fold improvement in potency (Figure 5A). To check whether FFY incorporation affected the initial binding affinity of mNb6, we measured the initial binding affinity of mNb6(WT) or mNb6(108FFY) toward the spike RBD by using biolayer interferometry (BLI). The timescale of the binding experiments (50 s for the association step) was faster than the timescale for covalent-bond formation, so we could measure the initial binding affinity of mNb6(108FFY) toward the spike RBD without a covalent-bonding effect. The K_D was measured to be 0.85 ± 0.19 nM for mNb6(WT) and 0.91 ± 0.11 nM for mNb6(108FFY) (Figures 5B and 5C), which were not significantly different, indicating that FFY incorporation did not significantly affect mNb6 initial binding affinity. Therefore, the drastically elevated potency of mNb6(108FFY) over mNb6(WT) in neutralizing pseudovirus infection should be attributed not to the difference in initial affinity but to the effect of covalent binding.

Encouraged by the highly potent effect on SARS-CoV-2 pseudovirus, we further tested the neutralizing efficacy of mNb6(108FFY) on authentic SARS-CoV-2 virus (Figure 5D). We incubated nanoluciferase-encoding SARS-CoV-2 with the nanobodies at 37°C for 1 h and then added the virus-nanobody mixtures to 293T-ACE2 cells for 2 h to allow infection. 72 h after infection, we measured luciferase signal in cells to determine the level of infection. As shown in Figure 5E, the IC_{50} of mNb6(WT) in inhibiting authentic SARS-CoV-2 was 69.9 nM, whereas the IC_{50} measured for mNb6(108FFY) was 1.7 nM, indicating a drastic 41-fold improvement in potency.

mNb6(108FFY) covalently binds and potently inhibits certain SARS-CoV-2 variants

Various mutated SARS-CoV-2 strains have emerged during the pandemic. The B.1.1.7 variant (Alpha), which possesses the N501Y mutation, shows a stronger interaction with ACE2 and a faster spreading rate;[30,31] the B.1.351 variant (Beta), which possesses K417N, E484K, and N501Y mutations on the RBD, has a decreased affinity toward neutralization antibodies and can lower the effectiveness of the current vaccine.[13,14,32,33] The B.1.617.2 variant (Delta), which has the L452R and T478K mutations on the RBD, has increased transmissibility and is less sensitive to monoclonal antibodies and neutralizing antibodies from recovered individuals, as well as vaccine-elicited antibodies.[15,34,35] More recently, the B.1.1.529 (Omicron) variants,

Please cite this article in press as: Yu et al., Accelerating PERx reaction enables covalent nanobodies for potent neutralization of SARS-CoV-2 and variants, Chem (2022), https://doi.org/10.1016/j.chempr.2022.07.012

which have much elevated immune evasion, have become the dominant strains in many countries and spread more easily than earlier variants.[36,37]

We first tested whether the variants would escape from mNb6(WT) binding. BLI measurement showed that mNb6 had a decreased binding affinity toward the RBD of the Alpha and Delta variants. The K_D of mNb6(WT) with the Alpha and Delta RBD was 1.50 $\pm$ 0.05 and 8.6 $\pm$ 1.7 nM, respectively (Figures 5F and 5G), significantly higher than 0.85 nM, the K_D with the WT RBD. In contrast, mNb6(WT) did not show significant binding with the Beta RBD up to a concentration of 50 nM (Figure S6). We next determined whether mNb6(108FFY) could cross-link the RBD of various variants. Western blot analysis indicated that mNb6(108FFY) efficiently cross-linked with the Delta and Alpha RBD (Figure 5H; quantification in Figure S7), although the cross-linking rate (k_{obs} = 0.156 $\pm$ 0.036 h^{-1} for Delta and 0.086 $\pm$ 0.008 h^{-1} for Alpha) was slightly slower than that with the WT RBD (k_{obs} = 0.244 $\pm$ 0.031 h^{-1}), consistent with the decreased affinity toward these variants. For the Beta RBD, although the affinity was dramatically reduced, mNb6(108FFY) was still able to cross-link it, albeit in low efficiency (~5%) (Figure 5H). We also found that mNb6(WT) had a lower binding affinity toward the spike RBD of the Epsilon variant (K_D = 1.32 $\pm$ 0.11 nM) and the Lambda variant (K_D = 2.86 $\pm$ 0.77 nM) than the WT SARS-CoV-2 and that mNb6(108FFY) could efficiently cross-link the spike RBD of these two variants (Figures S8A–S8D). These results demonstrate that the covalent mNb6(108FFY) was capable of cross-linking the spike RBD of the SARS-Cov-2 variants as long as the variant did not completely abolish binding with mNb6.

We further assessed the efficacy of mNb6(108FFY) in neutralizing pseudovirus of SARS-CoV-2 variants, to which mNb6(WT) did not abolish binding. The IC_{50} of mNb6(WT) in inhibiting the Alpha variant pseudovirus was 36.5 nM (Figure 5I), whereas mNb6(108FFY) had an IC_{50} of 1.6 nM, showing a 23-fold increase in potency. For the quickly spreading Delta variant, mNb6(WT) inhibited the pseudovirus with an IC_{50} of 143 nM (Figure 5J), whereas mNb6(108FFY) was able to neutralize the Delta variant pseudovirus with an IC_{50} of 3.7 nM to achieve a 39-fold improvement in potency. For the Epsilon variant pseudovirus, mNb6(WT) inhibited it with an IC_{50} of 304 nM, whereas mNb6(108FFY) inhibited it with an IC_{50} of 8.03 nM, exhibiting 38-fold increase in potency (Figure S8E). Similarly, mNb6(108FFY) gained a 24-fold increase in potency in inhibiting the Lambda variant pseudovirus (IC_{50} = 12.4 nM) over the mNb6(WT) (IC_{50} = 299 nM) (Figure S8F). In sum, the covalent mNb6(108FFY) nanobody potently inhibited the Alpha, Delta, Epsilon, and Lambda variant pseudoviruses, showing remarkable higher potency than the mNb6(WT) nanobody (Figure 5K).

The large number of mutations (15 in the BA.1 RBD) in Omicron variants abolished the binding of nanobody mNb6 and thus the cross-linking between mNb6(108FFY) and the Omicron RBD (Figure S9). We therefore used a different nanobody (Nb70) capable of binding with Omicron variants by contacting two RBDs in their up state.[38] We decided to incorporate FSY at site G56, Y103, or D115 of nanobody Nb70 according to the crystal structure[38] to target the K386, Y369, or K378 site of the spike RBD, respectively (Figure S10A). All three sites in Nb70, after FSY incorporation, allowed efficient covalent cross-linking of both the Omicron BA.1 and BA.2 spike RBDs (Figure S10B). We chose site 56 for further studies because its protein yields (2.5 mg/L) were higher than those of the two other sites. We then used FFY for the following studies because its kinetics were faster than those of FSY. MS analysis of the intact protein confirmed that FFY was incorporated into Nb70 at site 56 in high fidelity (Figure S10C). We next verified that FFY incorporation at site 56

Please cite this article in press as: Yu et al., Accelerating PERx reaction enables covalent nanobodies for potent neutralization of SARS-CoV-2 and variants, Chem (2022), https://doi.org/10.1016/j.chempr.2022.07.012

permitted fast cross-linking of Nb70(56FFY) with both the BA.1 and BA.2 RBDs (Figures S10D and S10E) such that cross-linking showed up in 5 min. The binding affinity of Nb70 toward the BA.1 spike RBD was measured to be 0.14 nM. Besides Omicron, Nb70(56FFY) was also shown to cross-link with the spike RBD from various other variants, including Alpha, Beta, Delta, and Lambda (Figure S10F). Lastly, we measured the IC_{50}s of Nb70(WT) and Nb70(56FFY) in inhibiting the Omicron BA.1 variant and the Omicron BA.2 variant pseudovirus (Figures S10G and S10H) and found that the potency of Nb70(56FFY) increased 10-fold for BA.1 and 8.1-fold for BA.2 over Nb70(WT). These results indicate that covalent nanobody Nb70(56FFY) could also inhibit the Omicron variants more potently than the WT Nb70.

Engineering human ACE2 receptor into an irreversible covalent binder for SARS-CoV-2

In addition to engineering artificial nanobodies specific to the spike RBD, we also sought to engineer the native receptor, human ACE2, into a covalent binder to block the interaction between the SARS-CoV-2 spike protein and human ACE2. Using a soluble ACE2 receptor binding to the viral spike protein, thereby neutralizing SARS-CoV-2, is an attractive strategy. The spike protein of SARS-CoV-2 binds to the ACE2 receptor with a K_D of 4.7 nM,[39] comparable to affinities of monoclonal antibodies. In addition, ACE2 administration could additionally treat pneumonia caused by SARS-CoV-2. Coronavirus binding leads to ACE2 shedding and downregulation, which induces pulmonary edema and acute respiratory distress syndrome (ARDS). Administration of recombinant human ACE2 (rhACE2) improves acute lung injury and reduces ARDS in preclinical studies.[40,41] Moreover, rhACE2 is safe and well tolerated by patients in phase II trials,[42,43] and small levels of soluble ACE2 are secreted and circulate in the human body.[44] More importantly, the soluble ACE2 therapy is expected to have broad coverage given that SARS-CoV-2 cannot escape ACE2 neutralization because of its dependence on the same protein for cell entry. Any mutation that reduces SARS-CoV-2's affinity for the ACE2-based therapeutics will render the virus less pathogenic.

To this end, we explored whether the soluble human ACE2 could be engineered into a covalent binder for the SARS-CoV-2 spike protein. On the basis of the crystal structure of the SARS-CoV-2 spike RBD in complex with human ACE2 (Figure 6A),[39] we decided to incorporate FSY at site D30, H34, E37, D38, Q42, or Y83 to target the proximal nucleophilic amino acid residues on the spike RBD. We expressed and purified these FSY-incorporated ACE2 mutant proteins from HEK293 cells, individually incubated them with the spike RBD, and then performed western blot analysis (Figure 6B). Cross-linking of ACE2(FSY) with the spike RBD was detected when FSY was incorporated at site 34, 37, or 42. The ACE2 (34FSY) mutant exhibited the highest cross-linking efficiency (28.3%). The cross-linking kinetic experiments of ACE2(FSY) with the spike RBD showed that cross-linking was detectable at 1 h and increased with incubation time (Figure 6C). Furthermore, we analyzed the cross-linking product of ACE2(34FSY) with the spike RBD by using high-resolution MS, which clearly indicated that FSY of ACE2(34FSY) specifically reacted with K417 of the spike RBD (Figure S11), as designed according to the crystal structure. Because K417 is mutated in some variants, we tested the cross-linking of ACE2(34FSY) with the spike RBD of different variants. ACE2(34FSY) did not cross-link with the Beta or Omicron spike RBD, each of which has the K417N mutation. On the other hand, ACE2(34FSY) cross-linked with the Alpha and Delta spike RBDs, which do not have a mutation at K417, in high efficiency (Figure 6D). These results together show that ACE2(34FSY) covalently bound to the spike RBD through targeting K417 specifically. To address variants harboring the K417 mutation, one could screen more sites

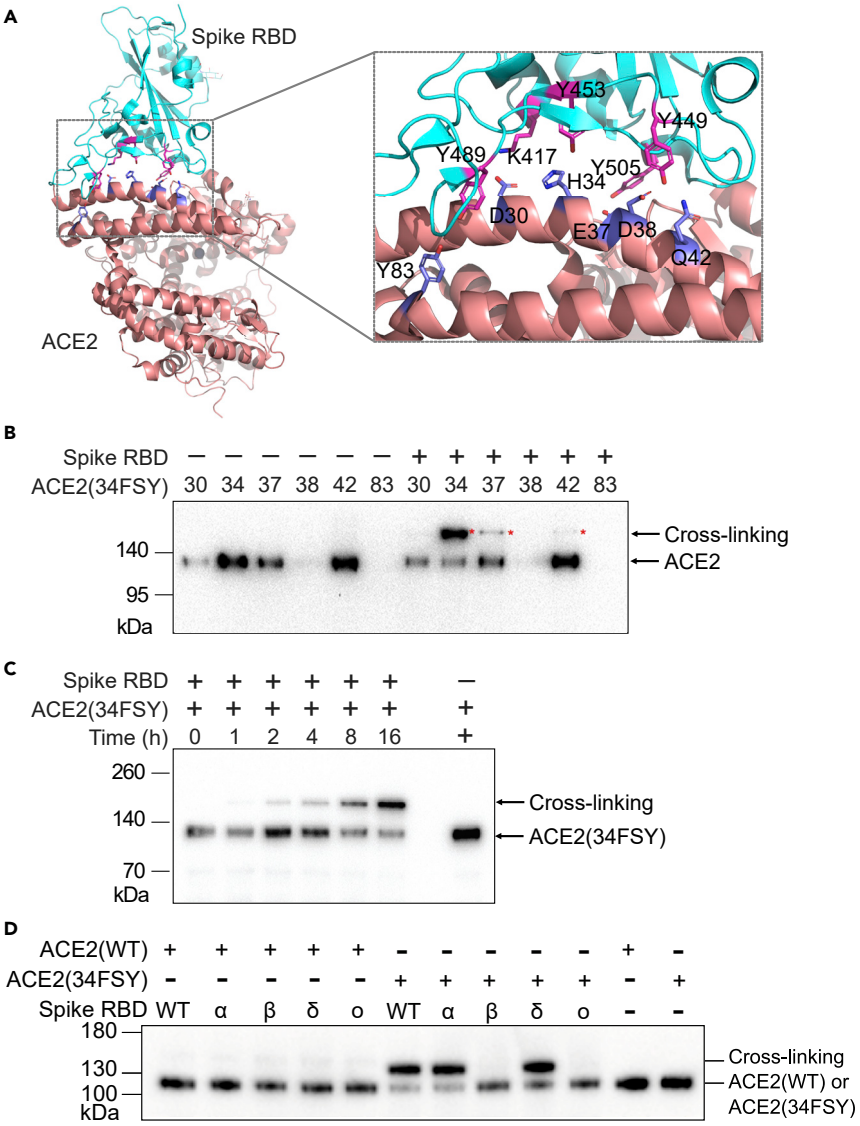

Figure 6. Engineering soluble human ACE2 to covalently bind to the SARS-CoV-2 spike protein

(A) Crystal structure of the SARS-CoV-2 spike RBD bound with human ACE2 (PDB: 6M0J). Sites on ACE2 selected to incorporate FSY are shown in blue sticks, and target residues on the spike RBD are shown in magenta sticks.

(B) Western blot analysis of cross-linking of the spike RBD with soluble human ACE2 and its FSY mutants at 37°C. An antibody against the Hisx6 tag at the C terminus of ACE2(FSY) was used for detection.

(C) Western blot analysis of ACE2(34FSY) (0.16 μM) cross-linking with the spike RBD (0.57 μM) at the indicated time duration. An antibody against the Hisx6 tag at the C terminus of ACE2(FSY) was used for detection.

(D) ACE2(34FSY) also cross-linked with the spike RBD of the Alpha and Delta variants but not the Beta or Omicron variant.

See also Figure S11.

on ACE2 for FSY incorporation to covalently target residues other than K417 on the spike RBD. Alternatively, we have shown covalent nanobodies such as Nb70(56FFY) could efficiently cross-link with the Beta and Omicron RBDs (Figures S10D–S10F) to overcome the K417 mutation by targeting other residues.

Please cite this article in press as: Yu et al., Accelerating PERx reaction enables covalent nanobodies for potent neutralization of SARS-CoV-2 and variants, Chem (2022), https://doi.org/10.1016/j.chempr.2022.07.012

DISCUSSION

In summary, through genetic incorporation of the latent bioreactive Uaas FSY and FFY into nanobodies, we have generated multiple covalent nanobodies that bind with the spike RBD of SARS-CoV-2 irreversibly via the PERx mechanism. The freshly developed FFY increased the PERx reaction rate by 2.4-fold over the original FSY, and the resultant covalent nanobody, mNb6(108FFY), efficiently neutralized both SARS-CoV-2 pseudovirus and authentic SARS-CoV-2, increasing the potency by a drastic 36- and 41-fold, respectively, over the noncovalent WT mNb6. In addition, the covalent mNb6(108FFY) nanobody also potently inhibited the Alpha, Delta, Epsilon, and Lambda variants of SARS-CoV-2 pseudovirus with 23-, 39-, 38-, and 24-fold higher potency, respectively, than the WT mNb6. Similarly, the covalent nanobody Nb70(56FFY) inhibited the Omicron BA.1 and BA.2 variants more potently than the WT Nb70 with 10- and 8.1-fold increased potency, respectively. Moreover, using a similar strategy, we also engineered the soluble human ACE2 receptor into a covalent binder that irreversibly cross-links with the spike RBD via PERx.

Our results demonstrate that nanobodies can be readily engineered into covalent binders through the incorporation of a latent bioreactive Uaa, which reacts with a natural residue of the target protein only upon nanobody-target binding, expanding the scope of PERx, which we previously developed and applied to the immune-checkpoint PD-1/PD-L1.[20,21] We identified nanobody sites appropriate for FSY or FFY incorporation and cross-linking either by inspecting the structure of the nanobody-target complex[45] or by simply screening all sites in the nanobody's three CDRs. Recent breakthroughs in the accurate prediction of protein structure and interactions have made structural information available for a broad range of proteins,[46,47] which will greatly facilitate structure-guided site identification. On the other hand, there are about 30 total sites in the nanobody's three CDRs, screening of which using cross-linking and western blot analysis can be completed in less than 2 weeks. Unbiased screening could identify cross-linking sites that are not obvious by simple checking of the structure. We have always identified multiple sites in diverse nanobodies with successful cross-linking because of FSY's and FFY's exceptional ability to react with multiple residues, including Tyr, His, and Lys,[25] which are often found at the protein-protein interface. To access more target sites, we have also developed FSK (which has a longer and more flexible side chain to reach residues at further distances) and mFSY to reach residues with different side-chain orientations.[45,48] These site-identification strategies are straightforward and obviate sophisticated instrumentation such as MS and should be generally applicable to engineering various proteins—such as antibodies, Fab,[48] single-chain variable fragment (ScFv), affibodies,[20] and DARPins—into covalent binders.

Compared with conventional noncovalent drugs, drugs working in covalent mode offer desirable features such as increased potency, prolonged duration, and the possibility to prevent drug resistance, as demonstrated with covalent small-molecule drugs.[16] Here, we have demonstrated that covalent nanobodies, representing covalent protein drugs, possess similar valuable properties as well. In particular, the covalent mNb6(108FFY) drastically increased the potency over WT mNb6 to 36-fold in inhibiting SARS-CoV-2 pseudovirus and to 41-fold in inhibiting authentic SARS-CoV-2. Aside from the WT SARS-CoV-2, mNb6(108FFY) was also able to covalently cross-link and neutralize the Alpha, Delta, Epsilon, and Lambda variants of SARS-CoV-2 with a potency increase ranging from 23- to 39-fold over the WT mNb6. We

Please cite this article in press as: Yu et al., Accelerating PERx reaction enables covalent nanobodies for potent neutralization of SARS-CoV-2 and variants, Chem (2022), https://doi.org/10.1016/j.chempr.2022.07.012

CellPress

measured these potency increases by incubating the nanobody with the virus for 1 h. Because the extent of covalent cross-linking increases with time, the potency of covalent nanobodies should be greater with longer incubation time.

A caveat of the PERx strategy is that the cross-linking rate can be negatively affected when the binding affinity between the protein drug and target decreases drastically as a result of target mutation, such as mNb6(108FFY) and the Beta RBD or Omicron RBD. In rare cases, mutation can even occur at the cross-linking residue, which would abolish cross-linking at that site; for example, ACE2(34FSY) did not cross-link the Beta RBD or Omicron RBD as a result of the K417N mutation. On the other hand, this feature ensures high specificity in cross-linking and thus avoids undesired nonspecific reaction with other proteins *in vivo*. As we demonstrated here and previously,[20,45] PERx is a general strategy that can be applied on diverse nanobodies, and each nanobody can have FFY incorporated at multiple sites to target different natural residues on the spike RBD to achieve cross-linking (Figure 3). Therefore, other nanobodies able to bind the mutated spike RBD could be similarly engineered, and diverse covalent nanobodies could be used in combination to ensure the cross-linking and inhibition of future potential variants. For instance, although mNb6(108FFY) could not efficiently target the Beta or Omicron variant covalently, we demonstrated that a different nanobody (Nb70(56FFY)) efficiently cross-linked with the Omicron BA.1 and BA.2 variants, the Beta variant, and the Alpha, Delta, and Lambda variants. When in use, the irreversible cross-linking ability and the multi-targeting of these covalent nanobodies have the potential for complete viral inhibition. Nonetheless, animal tests and clinical trials are warranted to confirm these potential benefits of covalent protein drugs, and nonspecific reactivity of covalent proteins *in vivo* should be carefully evaluated.

Fast reaction kinetics would be critical for effective inhibition of viral infection because they would enable covalent cross-links to promptly form between the protein drug and the target within a shorter contact time and to reach a higher extent for more effective neutralization. By introducing electron-withdrawing fluorine substitution, we designed and genetically encoded a unique latent bioreactive Uaa (FFY), which afforded a marked 2.4-fold increase in reaction rate in the cross-linking of mNb6 with the spike RBD over the original FSY. In a recent communication,[49] Han and co-workers exploited the FSY and PERx mechanism developed by us[20,25] and incorporated FSY into the spike-specific minibinders *de novo* designed by the Baker group.[8] The resultant FSY-minibinder required 2 h incubation to cross-link with the spike RBD *in vitro* and 2 h incubation with the virus to show a moderate 6-fold increase in potency in neutralizing a single SARS-CoV-2 variant. It is unclear whether the increased potency of the FSY-minibinder is general given that no neutralization of WT SARS-CoV-2 or other variants was demonstrated. The longer the incubation time required for the drug, the more likely the virus will gain access to human cells for infection. In stark contrast, our latest generation of FFY-enabled covalent nanobody mNb6(108FFY) exhibited robust cross-linking with the spike RBD within 10 min. We incubated mNb6(108FFY) with SARS-CoV-2 for a shorter 1 h and achieved a drastic 41-fold increase in potency in neutralizing SARS-CoV-2. In addition, we showed that mNb6(108FFY) also increased the potency in neutralizing the WT, Alpha, Delta, Epsilon, and Lambda variants of SARS-CoV-2 pseudovirus by 36-, 23-, 39-, 38-, and 24-fold, respectively, demonstrating that the increased potency of the covalent nanobody is robust and general. Therefore, fast reaction kinetics of FFY are critical to enhancing the potency of covalent protein drugs.

Our results indicate that covalently engineered nanobodies exhibit different potency increases over their WT nanobodies in viral neutralization. Several factors might contribute to this difference. First, the latent bioreactive Uaas were incorporated at different positions of different nanobodies for optimal cross-linking rates. As a result, different residues on the spike RBD were targeted. Second, SR4 binds with a single RBD, whereas both mNb6 and Nb70 bind with one RBD while straddling another RBD simultaneously (i.e., contacting two RBDs simultaneously). The latter is analogous to an antibody, which is bivalent and able to bind two antigens simultaneously. Bivalent binding by an antibody induces the desired conformational change and has been reported to modify the activity of leukocyte-function-associated antigen 1.[50] We note that other factors, such as the nanobody epitope on the RBD and the binding affinity, could also play a role. Our data were obtained from a limited number of nanobodies, and further work is warranted to conclude the mechanism.

Covalent nanobodies could lead to protein drugs that can be readily produced in large scale via bacterial expression, easily stored and distributed because of the nanobody's high stability, and aerosolized for self-administered inhalation to nasal and lung epithelia.[7] Further development could afford a medication for COVID-19 patients to prevent significant morbidities and death and provide a potential prophylactic to give passive immunity to clinical providers at the front line. In addition, the PERx-capable ACE2 drugs can serve as a therapeutic stockpile for future outbreaks of SARS-CoV, SARS-CoV-2, and any new coronavirus that uses the ACE2 receptor for entry. Moreover, through irreversible binding, covalent protein drugs can potentially achieve complete viral inhibition and mitigate viral resistance. Lastly, the principle of generating a covalent binder or a covalent soluble receptor inhibitor via PERx can be generally applied to the development of covalent protein drugs to effectively treat various other infectious diseases, such as influenza, hepatitis, AIDS, and anthrax.

EXPERIMENTAL PROCEDURES

Resource availability

Lead contact

Further information and requests for resources and reagents should be directed to and will be fulfilled by the lead contact, Lei Wang (lei.wang2@ucsf.edu).

Materials availability

Unique reagents generated in this study are available from the lead contact with a completed material transfer agreement.

Data and code availability

All data supporting this study are available within the main article and supplemental information. This study did not generate any datasets or original code.

SUPPLEMENTAL INFORMATION

Supplemental information can be found online at https://doi.org/10.1016/j.chempr.2022.07.012.

ACKNOWLEDGMENTS

L.W. acknowledges support from the UCSF Catalyst Award (7030487) and the National Institutes of Health (NIH) (R01CA258300). M.O. thanks the Rodenberry Foundation, NIH (R37AI083139), and Gladstone Institutes for their support.

Please cite this article in press as: Yu et al., Accelerating PERx reaction enables covalent nanobodies for potent neutralization of SARS-CoV-2 and variants, Chem (2022), https://doi.org/10.1016/j.chempr.2022.07.012

CellPress

AUTHOR CONTRIBUTIONS

B.Y. synthesized FFY, measured the cross-linking kinetics, determined the binding constant, and designed the experiments; S.L. screened Uaa incorporation sites in nanobodies, performed the pseudovirus assay and cross-linking of ACE2(34FSY) with variants, and designed the experiments; T.T. performed the authentic SARS-CoV-2 neutralization assay; N.W. screened Uaa incorporation sites in ACE2 and performed ACE2 cross-linking experiments; L.C. and W.S. constructed the Nb70 plasmids and purified Nb70 proteins; J.L. analyzed the MS data; G.R.K. and M.O. designed and supervised the authentic SARS-CoV-2 neutralization assay; L.W. conceived and supervised the whole project; L.W., B.Y., and S.L. wrote the manuscript; and all authors discussed the results and commented on the manuscript.

DECLARATION OF INTERESTS

L.W., B.Y., S.L., and N.W. are inventors on a patent application related to this work.

Received: March 9, 2022
Revised: June 22, 2022
Accepted: July 14, 2022
Published: July 17, 2022

REFERENCES

1. Zhou, P., Yang, X.-L., Wang, X.-G., Hu, B., Zhang, L., Zhang, W., Si, H.-R., Zhu, Y., Li, B., Huang, C.-L., et al. (2020). A pneumonia outbreak associated with a new coronavirus of probable bat origin. Nature *579*, 270–273.

2. Kyriakidis, N.C., López-Cortés, A., González, E.V., Grimaldos, A.B., and Prado, E.O. (2021). SARS-CoV-2 vaccines strategies: A comprehensive review of phase 3 candidates. NPJ Vaccines *6*, 28.

3. Hoffmann, M., Kleine-Weber, H., Schroeder, S., Krüger, N., Herrler, T., Erichsen, S., Schiergens, T.S., Herrler, G., Wu, N.-H., Nitsche, A., et al. (2020). SARS-CoV-2 cell entry depends on ACE2 and TMPRSS2 and is blocked by a clinically proven protease inhibitor. Cell *181*, 271–280.e8.

4. Jackson, C.B., Farzan, M., Chen, B., and Choe, H. (2022). Mechanisms of SARS-CoV-2 entry into cells. Nat. Rev. Mol. Cell Biol. *23*, 3–20.

5. Xiu, S., Dick, A., Ju, H., Mirzaie, S., Abdi, F., Cocklin, S., Zhan, P., and Liu, X. (2020). Inhibitors of SARS-CoV-2 entry: Current and future opportunities. J. Med. Chem. *63*, 12256–12274.

6. Wu, Y., Wang, F., Shen, C., Peng, W., Li, D., Zhao, C., Li, Z., Li, S., Bi, Y., Yang, Y., et al. (2020). A noncompeting pair of human neutralizing antibodies block COVID-19 virus binding to its receptor ACE2. Science *368*, 1274–1278.

7. Schoof, M., Faust, B., Saunders, R.A., Sangwan, S., Rezelj, V., Hoppe, N., Boone, M., Billesbølle, C.B., Puchades, C., Azumaya, C.M., et al. (2020). An ultrapotent synthetic nanobody neutralizes SARS-CoV-2 by stabilizing inactive spike. Science *370*, 1473–1479.

8. Cao, L., Goreshnik, I., Coventry, B., Case, J.B., Miller, L., Kozodoy, L., Chen, R.E., Carter, L., Walls, A.C., Park, Y.-J., et al. (2020). De novo design of picomolar SARS-CoV-2 miniprotein inhibitors. Science *370*, 426–431.

9. Bojadzic, D., Alcazar, O., Chen, J., Chuang, S.-T., Condor Capcha, J.M., Shehadeh, L.A., and Buchwald, P. (2021). Small-molecule inhibitors of the coronavirus spike: ACE2 protein-protein interaction as blockers of viral attachment and entry for SARS-CoV-2. ACS Infect. Dis. *7*, 1519–1534.

10. Larue, R.C., Xing, E., Kenney, A.D., Zhang, Y., Tuazon, J.A., Li, J., Yount, J.S., Li, P.-K., and Sharma, A. (2021). Rationally designed ACE2-derived peptides inhibit SARS-CoV-2. Bioconjug. Chem. *32*, 215–223.

11. Sun, M., Liu, S., Wei, X., Wan, S., Huang, M., Song, T., Lu, Y., Weng, X., Lin, Z., Chen, H., et al. (2021). Aptamer blocking strategy inhibits SARS-CoV-2 virus infection. Angew. Chem. Int. Ed. Engl. *60*, 10266–10272.

12. Bracken, C.J., Lim, S.A., Solomon, P., Rettko, N.J., Nguyen, D.P., Zha, B.S., Schaefer, K., Byrnes, J.R., Zhou, J., Lui, I., et al. (2021). Bi-paratopic and multivalent VH domains block ACE2 binding and neutralize SARS-CoV-2. Nat. Chem. Biol. *17*, 113–121.

13. Wang, P., Nair, M.S., Liu, L., Iketani, S., Luo, Y., Guo, Y., Wang, M., Yu, J., Zhang, B., Kwong, P.D., et al. (2021). Antibody resistance of SARS-CoV-2 variants B.1.351 and B.1.1.7. Nature *593*, 130–135.

14. Planas, D., Bruel, T., Grzelak, L., Guivel-Benhassine, F., Staropoli, I., Porrot, F., Planchais, C., Buchrieser, J., Rajah, M.M., Bishop, E., et al. (2021). Sensitivity of infectious SARS-CoV-2 B.1.1.7 and B.1.351 variants to neutralizing antibodies. Nat. Med. *27*, 917–924.

15. Mlcochova, P., Kemp, S.A., Dhar, M.S., Papa, G., Meng, B., Ferreira, I.A.T.M., Datir, R., Collier, D.A., Albecka, A., Singh, S., et al. (2021). SARS-CoV-2 B.1.617.2 Delta variant replication and immune evasion. Nature *599*, 114–119.

16. Singh, J., Petter, R.C., Baillie, T.A., and Whitty, A. (2011). The resurgence of covalent drugs. Nat. Rev. Drug Discov. *10*, 307–317.

17. Bauer, R.A. (2015). Covalent inhibitors in drug discovery: From accidental discoveries to avoided liabilities and designed therapies. Drug Discov. Today *20*, 1061–1073.

18. Xiang, Z., Ren, H., Hu, Y.S., Coin, I., Wei, J., Cang, H., and Wang, L. (2013). Adding an unnatural covalent bond to proteins through proximity-enhanced bioreactivity. Nat. Methods *10*, 885–888.

19. Wang, L. (2017). Genetically encoding new bioreactivity. N. Biotechnol. *38*, 16–25.

20. Li, Q., Chen, Q., Klauser, P.C., Li, M., Zheng, F., Wang, N., Li, X., Zhang, Q., Fu, X., Wang, Q., et al. (2020). Developing covalent protein drugs via proximity-enabled reactive therapeutics. Cell *182*, 85–97.e16.

21. Cao, L., and Wang, L. (2022). New covalent bonding ability for proteins. Protein Sci. *31*, 312–322.

22. Wang, L., Brock, A., Herberich, B., and Schultz, P.G. (2001). Expanding the genetic code of *Escherichia coli*. Science *292*, 498–500.

23. Huo, J., Le Bas, A., Ruza, R.R., Duyvesteyn, H.M.E., Mikolajek, H., Malinauskas, T., Tan, T.K., Rijal, P., Dumoux, M., Ward, P.N., et al. (2020). Neutralizing nanobodies bind SARS-CoV-2 spike RBD and block interaction with ACE2. Nat. Struct. Mol. Biol. *27*, 846–854.

24. Li, T., Cai, H., Yao, H., Zhou, B., Zhang, N., van Vlissingen, M.F., Kuiken, T., Han, W., GeurtsvanKessel, C.H., Gong, Y., et al. (2021). A synthetic nanobody targeting RBD protects hamsters from SARS-CoV-2 infection. Nat. Commun. *12*, 4635.

Please cite this article in press as: Yu et al., Accelerating PERx reaction enables covalent nanobodies for potent neutralization of SARS-CoV-2 and variants, Chem (2022), https://doi.org/10.1016/j.chempr.2022.07.012

25. Wang, N., Yang, B., Fu, C., Zhu, H., Zheng, F., Kobayashi, T., Liu, J., Li, S., Ma, C., Wang, P.G., et al. (2018). Genetically encoding fluorosulfate-L-tyrosine to react with lysine, histidine, and tyrosine via SuFEx in proteins in vivo. J. Am. Chem. Soc. *140*, 4995–4999.

26. Xu, J., Xu, K., Jung, S., Conte, A., Lieberman, J., Muecksch, F., Lorenzi, J.C.C., Park, S., Schmidt, F., Wang, Z., et al. (2021). Nanobodies from camelid mice and llamas neutralize SARS-CoV-2 variants. Nature *595*, 278–282.

27. Crawford, K.H.D., Eguia, R., Dingens, A.S., Loes, A.N., Malone, K.D., Wolf, C.R., Chu, H.Y., Tortorici, M.A., Veesler, D., Murphy, M., et al. (2020). Protocol and reagents for pseudotyping lentiviral particles with SARS-CoV-2 spike protein for neutralization assays. Viruses *12*, 513.

28. Mukherjee, H., Debreczeni, J., Breed, J., Tentarelli, S., Aquila, B., Dowling, J.E., Whitty, A., and Grimster, N.P. (2017). A study of the reactivity of S(VI)-F containing warheads with nucleophilic amino-acid side chains under physiological conditions. Org. Biomol. Chem. *15*, 9685–9695.

29. Zhou, H., Mukherjee, P., Liu, R., Evrard, E., Wang, D., Humphrey, J.M., Butler, T.W., Hoth, L.R., Sperry, J.B., Sakata, S.K., et al. (2018). Introduction of a crystalline, shelf-stable reagent for the synthesis of sulfur(VI) fluorides. Org. Lett. *20*, 812–815.

30. Nelson, G., Buzko, O., Spilman, P., Niazi, K., Rabizadeh, S., and Soon-Shiong, P. (2021). Molecular dynamic simulation reveals E484K mutation enhances spike RBD-ACE2 affinity and the combination of E484K, K417N and N501Y mutations (501Y.V2 variant) induces conformational change greater than N501Y mutant alone, potentially resulting in an escape mutant. Preprint at bioRxiv. https://doi.org/10.1101/2021.01.13.426558.

31. Tian, F., Tong, B., Sun, L., Shi, S., Zheng, B., Wang, Z., Dong, X., and Zheng, P. (2021). N501Y mutation of spike protein in SARS-CoV-2 strengthens its binding to receptor ACE2. eLife *10*, e69091.

32. Madhi, S.A., Baillie, V., Cutland, C.L., Voysey, M., Koen, A.L., Fairlie, L., Padayachee, S.D., Dheda, K., Barnabas, S.L., Bhorat, Q.E., et al. (2021). Efficacy of the ChAdOx1 nCoV-19 Covid-19 vaccine against the B.1.351 variant. N. Engl. J. Med. *384*, 1885–1898.

33. Liu, Y., Liu, J., Xia, H., Zhang, X., Fontes-Garfias, C.R., Swanson, K.A., Cai, H., Sarkar, R., Chen, W., Cutler, M., et al. (2021). Neutralizing activity of BNT162b2-elicited serum. N. Engl. J. Med. *384*, 1466–1468.

34. Edara, V.-V., Pinsky, B.A., Suthar, M.S., Lai, L., Davis-Gardner, M.E., Floyd, K., Flowers, M.W., Wrammert, J., Hussaini, L., Ciric, C.R., et al. (2021). Infection and vaccine-induced neutralizing-antibody responses to the SARS-CoV-2 B.1.617 variants. N. Engl. J. Med. *385*, 664–666.

35. Allen, H., Vusirikala, A., Flannagan, J., Twohig, K.A., Zaidi, A., Chudasama, D., Lamagni, T., Groves, N., Turner, C., Rawlinson, C., et al. (2022). Household transmission of COVID-19 cases associated with SARS-CoV-2 Delta variant (B.1.617.2): National case-control study. Lancet Reg. Health Eur. *12*, 100252.

36. Cao, Y., Wang, J., Jian, F., Xiao, T., Song, W., Yisimayi, A., Huang, W., Li, Q., Wang, P., An, R., et al. (2022). Omicron escapes the majority of existing SARS-CoV-2 neutralizing antibodies. Nature *602*, 657–663.

37. Liu, L., Iketani, S., Guo, Y., Chan, J.F.-W., Wang, M., Liu, L., Luo, Y., Chu, H., Huang, Y., Nair, M.S., et al. (2022). Striking antibody evasion manifested by the Omicron variant of SARS-CoV-2. Nature *602*, 676–681.

38. Li, M., Ren, Y., Aw, Z.Q., Chen, B., Yang, Z., Lei, Y., Cheng, L., Liang, Q., Hong, J., Yang, Y., et al. (2022). Broadly neutralizing and protective nanobodies against diverse sarbecoviruses. Preprint at bioRxiv. https://doi.org/10.1101/2022.04.12.488087.

39. Lan, J., Ge, J., Yu, J., Shan, S., Zhou, H., Fan, S., Zhang, Q., Shi, X., Wang, Q., Zhang, L., and Wang, X. (2020). Structure of the SARS-CoV-2 spike receptor-binding domain bound to the ACE2 receptor. Nature *581*, 215–220.

40. Imai, Y., Kuba, K., Rao, S., Huan, Y., Guo, F., Guan, B., Yang, P., Sarao, R., Wada, T., Leong-Poi, H., et al. (2005). Angiotensin-converting enzyme 2 protects from severe acute lung failure. Nature *436*, 112–116.

41. Gu, H., Xie, Z., Li, T., Zhang, S., Lai, C., Zhu, P., Wang, K., Han, L., Duan, Y., Zhao, Z., et al. (2016). Angiotensin-converting enzyme 2 inhibits lung injury induced by respiratory syncytial virus. Sci. Rep. *6*, 19840.

42. Haschke, M., Schuster, M., Poglitsch, M., Loibner, H., Salzberg, M., Bruggisser, M., Penninger, J., and Krähenbühl, S. (2013). Pharmacokinetics and pharmacodynamics of recombinant human angiotensin-converting enzyme 2 in healthy human subjects. Clin. Pharmacokinet. *52*, 783–792.

43. Khan, A., Benthin, C., Zeno, B., Albertson, T.E., Boyd, J., Christie, J.D., Hall, R., Poirier, G., Ronco, J.J., Tidswell, M., et al. (2017). A pilot clinical trial of recombinant human angiotensin-converting enzyme 2 in acute respiratory distress syndrome. Crit. Care *21*, 234.

44. Shao, Z., Shrestha, K., Borowski, A.G., Kennedy, D.J., Epelman, S., Thomas, J.D., and Tang, W.H.W. (2013). Increasing serum soluble angiotensin-converting enzyme 2 activity after intensive medical therapy is associated with better prognosis in acute decompensated heart failure. J. Card. Fail. *19*, 605–610.

45. Liu, J., Cao, L., Klauser, P.C., Cheng, R., Berdan, V.Y., Sun, W., Wang, N., Ghelichkhani, F., Yu, B., Rozovsky, S., and Wang, L. (2021). A genetically encoded fluorosulfonyloxybenzoyl-L-lysine for expansive covalent bonding of proteins via SuFEx chemistry. J. Am. Chem. Soc. *143*, 10341–10351.

46. Jumper, J., Evans, R., Pritzel, A., Green, T., Figurnov, M., Ronneberger, O., Tunyasuvunakool, K., Bates, R., Žídek, A., Potapenko, A., et al. (2021). Highly accurate protein structure prediction with AlphaFold. Nature *596*, 583–589.

47. Baek, M., DiMaio, F., Anishchenko, I., Dauparas, J., Ovchinnikov, S., Lee, G.R., Wang, J., Cong, Q., Kinch, L.N., Schaeffer, R.D., et al. (2021). Accurate prediction of protein structures and interactions using a three-track neural network. Science *373*, 871–876.

48. Klauser, P.C., Berdan, V.Y., Cao, L., and Wang, L. (2022). Encoding latent SuFEx reactive meta-fluorosulfate tyrosine to expand covalent bonding of proteins. Chem. Commun. (Camb) *58*, 6861–6864.

49. Han, Y., Yang, Z., Hu, H., Zhang, H., Chen, L., Li, K., Kong, L., Wang, Q., Liu, B., Wang, M., et al. (2022). Covalently engineered protein minibinders with enhanced neutralization efficacy against escaping SARS-CoV-2 variants. J. Am. Chem. Soc. *144*, 5702–5707.

50. Grönholm, M., Jahan, F., Bryushkova, E.A., Madhavan, S., Aglialoro, F., Soto Hinojosa, L., Uotila, L.M., and Gahmberg, C.G. (2016). LFA-1 integrin antibodies inhibit leukocyte A4β1-mediated adhesion by intracellular signaling. Blood *128*, 1270–1281.